

N 70 15 16 4

NASA CR 107557

THE UNIVERSITY OF MICHIGAN
ANN ARBOR, MICHIGAN

SEMIANNUAL PROGRESS REPORT NO. 6

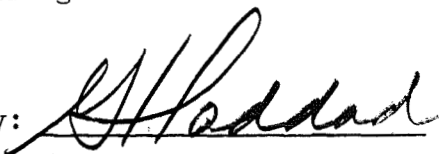
ON

MICROWAVE DEVICE INVESTIGATIONS

This report covers the period April 1, 1969 to October 1, 1969

Electron Physics Laboratory
Department of Electrical Engineering

By: W. R. Curtice
W. D. Getty
G. I. Haddad
R. J. Lomax

Approved by: 
G. I. Haddad, Director
Electron Physics Laboratory

Project 08400

RESEARCH GRANT NO. NGL 23-005-183
OFFICE OF SPACE SCIENCE AND APPLICATIONS
NATIONAL AERONAUTICS AND SPACE ADMINISTRATION
WASHINGTON, D. C. 20546

October, 1969

**CASE FILE
COPY**

TABLE OF CONTENTS

	<u>Page</u>
1. GENERAL INTRODUCTION	1
2. BEAM-PLASMA INTERACTIONS	1
2.1 Introduction	1
2.2 Conclusions	2
3. THE STUDY OF CYCLOTRON HARMONIC INSTABILITIES	2
3.1 Introduction	2
3.2 Velocity Distribution Measurements and Computations	2
3.3 Program for the Next Period	7
4. PARAMAGNETIC MATERIALS FOR MILLIMETER- AND SUBMILLIMETER-WAVE DETECTION	9
4.1 Introduction	9
4.2 Abstract of Forthcoming Technical Report	9
4.3 Program for the Next Period	11
5. BULK SEMICONDUCTOR MATERIALS FOR MILLIMETER- AND SUBMILLIMETER- WAVE DETECTION	11
6. MILLIMETER-WAVE GUNN-EFFECT DEVICES	12
6.1 Introduction	12
6.2 Dynamic Accumulation Layer	12
6.3 Dynamic-Domain Formation	13
6.4 Theoretical Results	18
6.5 Experimental Study	19
6.6 Conclusions	19
6.7 Program for the Next Period	19
7. ANALYSIS OF AVALANCHE-DIODE OSCILLATORS	19
7.1 Introduction	19

	<u>Page</u>
7.2 Analysis	21
7.3 Conclusions	21
7.4 Program for the Next Period	21

LIST OF ILLUSTRATIONS

<u>Figure</u>		<u>Page</u>
3.1	$f(v_z)$ vs. v_z at $B_o = 190$ G, $v_o = 576$ V and Corkscrew Current = 19 A.	4
3.2	(v_{\perp}/v_o) vs. z/L for Particles with Different Input Phase Angles χ_o .	5
3.3	Effect of Variation of Axial Magnetic Field Strength on Velocity Spread. (B_o is the Design Value of the Axial Field Strength and χ_o is the Input Phase Angle of the Particle.)	6
3.4	The Experimental Setup for the Study of Cyclotron Harmonic Waves.	8
6.1	Electric Field Configuration in the Model Crystal Showing the Anode, Cathode and Threshold Fields; E_A , E_C and E_{TH} , Respectively.	14
6.2	Average Electron Drift Velocities as a Function of Electric Field in the Anode and Cathode Sections of the Crystal.	15
6.3	Electric Field Configuration in the Model Crystal with a High-Field Domain Included.	16
6.4	Efficiency as a Function of n_o/f for Various Values of RF Field. Dc Bias Is 10 kV/cm, Doping Density Is $10^{15}/\text{cm}^3$ and the Crystal Length is 50 μm . The Curves Are Plotted for Doping Fluctuations of 1 and 3 Percent.	18

PAPERS PRESENTED DURING THE LAST PERIOD

C. F. Krumm and G. I. Haddad, "Millimeter- and Submillimeter-Wave Detection by Paramagnetic Materials," Presented at the 1969 IEEE G-MTT Int. Microwave Symposium, Dallas, Texas, May 1969.

G. T. Konrad and J. E. Rowe, "Harmonic Generation in Nonlinear Beam-Plasma Systems," Presented at the Third European Conf. on Controlled Fusion and Plasma Physics Symposium on Beam-Plasma Interactions, Utrecht, The Netherlands, June 1969.

SEMIANNUAL PROGRESS REPORT NO. 6

ON

MICROWAVE DEVICE INVESTIGATIONS

1. General Introduction (G. I. Haddad)

The purpose of this program is to investigate materials, devices and novel schemes for generation, amplification and detection of millimeter-wave energy. Several tasks are presently active under this program and the status of each one is described in the following sections of this report. Considerable progress has been made in the various tasks and several publications are presently being prepared. The tasks which were active during this report period are:

1. The study of cyclotron harmonic instabilities.
2. Paramagnetic materials for millimeter- and submillimeter-wave detection.
3. Bulk semiconductor materials for millimeter- and submillimeter-wave detection.
4. Millimeter-wave Gunn-effect devices.
5. Avalanche-diode oscillator analysis.

2. Beam-Plasma Interactions

Supervisor: R. J. Lomax

Staff: J. D. Gillanders

2.1 Introduction. The presence of gain or of an instability in a beam-plasma interaction can be determined by examining the dispersion equation of the interaction. Simplified theories which ignore collisions, finite temperature effects and some or all of the boundary conditions predict gain and instabilities much stronger than are observed experimentally. In the

simplest cases infinite gains are predicted. However, when the above factors are not ignored, the dispersion relation becomes much more complicated. Therefore, a very efficient method is needed to solve the equation if information about the interactions is to be obtained in a reasonable amount of computation time. A new approach to this problem has been outlined in previous reports.

2.2 Conclusions. The work on this topic has been completed and a technical report describing the results is currently being prepared. This should be completed in the near future. The work on this phase of the program will be terminated after the technical report is completed. This report will also be Mr. Gillander's' Ph.D. dissertation.

3. The Study of Cyclotron Harmonic Instabilities

Supervisor: W. D. Getty

Staff: A. Singh

3.1 Introduction. The objective of this phase of the project is the study of cyclotron harmonic instabilities in plasmas with anisotropic velocity distributions.

3.2 Velocity Distribution Measurements and Computations. The experimental work on the corkscrew device to be used in creating the required velocity distributions has been completed. Some typical results of such experiments were reported in the last semiannual progress report in the form of velocity analyzer current vs. retarding electrode potential plots. From such plots it is possible to construct a velocity distribution function for the beam and to estimate velocity spreads.

It can be shown that the z-velocity distribution of the beam is given by

$$f(v_z) = A \frac{dI}{dV_R} , \quad (3.1)$$

where $A =$ a constant,

$I =$ the analyzer collector current and

$V_R =$ the retarding electrode potential measured with respect to the cathode.

A typical plot of $f(v_z)$ vs. v_z obtained from experimental data is shown in Fig. 3.1. In obtaining data for this curve the axial magnetic field B_0 was adjusted to give a sharp cutoff of the beam analyzer collector current. Slight misadjustment of the value of B_0 causes severe velocity spreads.

These conclusions have been confirmed by studies on an analog computer (Applied Dynamics 2-64PB hybrid analog computer). Figures 3.2 and 3.3 show some of the results obtained from such studies. Assumptions made in modeling the equations of motion on the analog device are the same as those made by Wingerson et al.¹ Each curve in Fig. 3.2 shows the variation of v_{\perp}/v_0 vs. z/L for a specified input phase angle χ_0 . The angle χ_0 is the angular position of the particle measured with respect to the direction of the maximum of the radial magnetic field. All the other parameters (B_0 , v_0 , corkscrew current) are held at their design values. It can be seen from Fig. 3.2 that a large spread in v_{\perp}/v_0 is obtained at $z = L$.

Figure 3.3 shows the effect of variation of the axial magnetic field on compression of the velocity spread. Each curve portrays the variation of v_{\perp}/v_0 vs. z/L for two electrons launched at two widely different phase angles at the input to the corkscrew. The curves 1 and 2 are for the case when the magnetic field B_0 is set equal to the design value. Their transverse velocities at the output of the corkscrew are seen to be in the ratio of 1:2.

1. Wingerson, R. C., Dupree, T. H. and Rose, D. J., "Trapping and Loss of Charged Particles in a Perturbed Magnetic Field," Phys. Fluids, vol. 7, No. 9, pp. 1475-1484, September 1964.

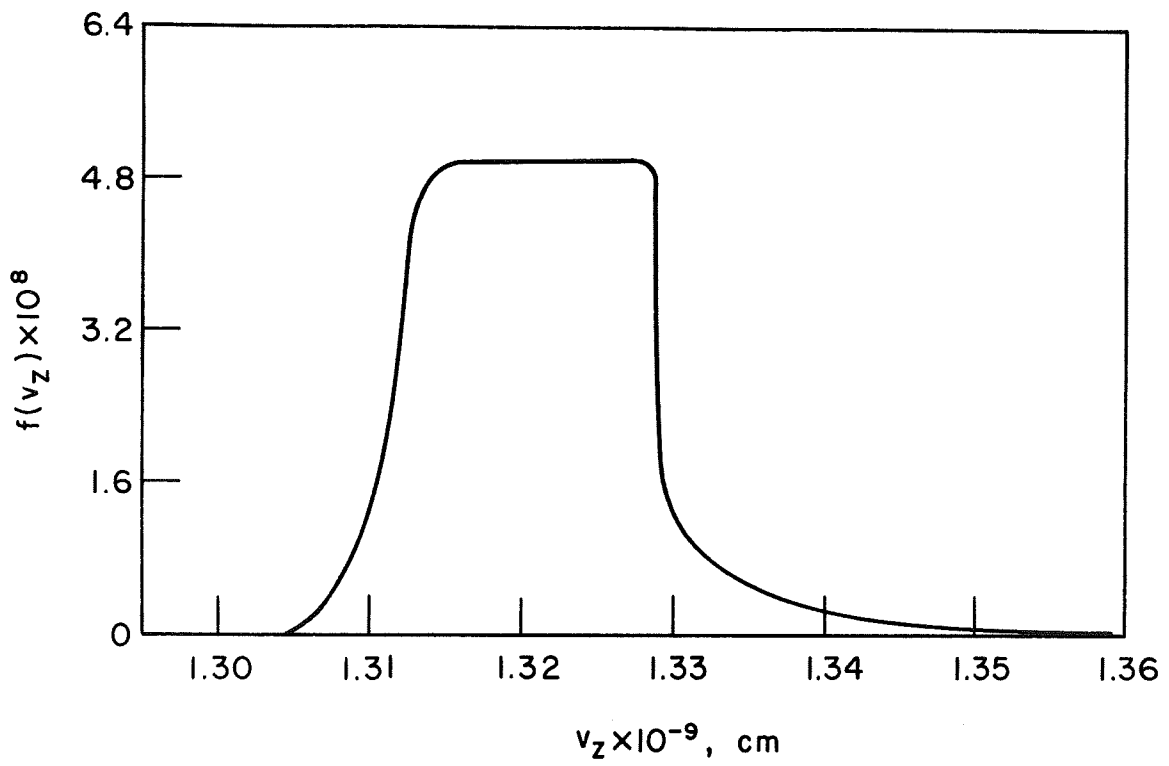


FIG. 3.1 $f(v_z)$ VS. v_z at $B_0 = 190$ G, $v_0 = 576$ V AND
CORKSCREW CURRENT = 19 A.

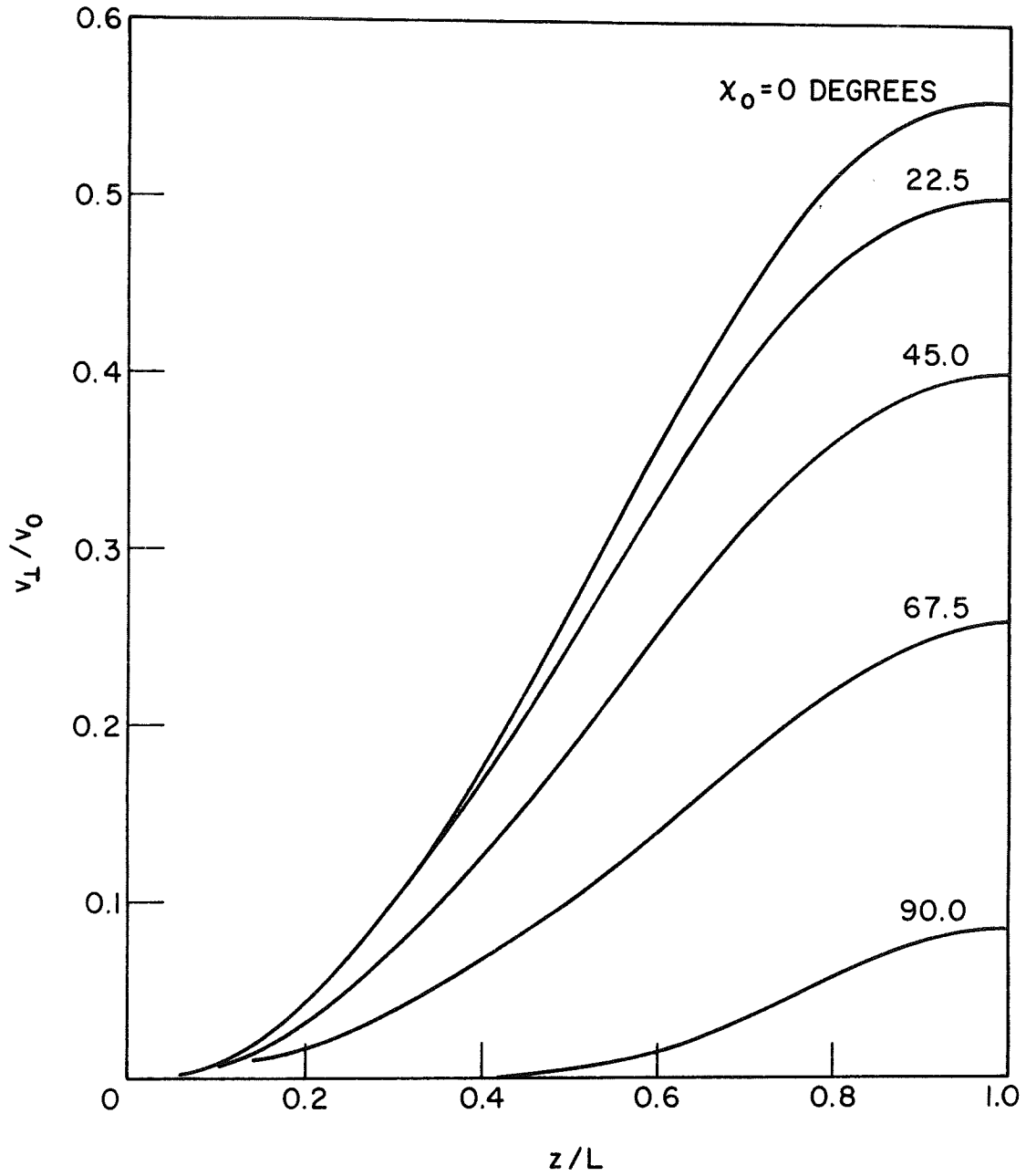
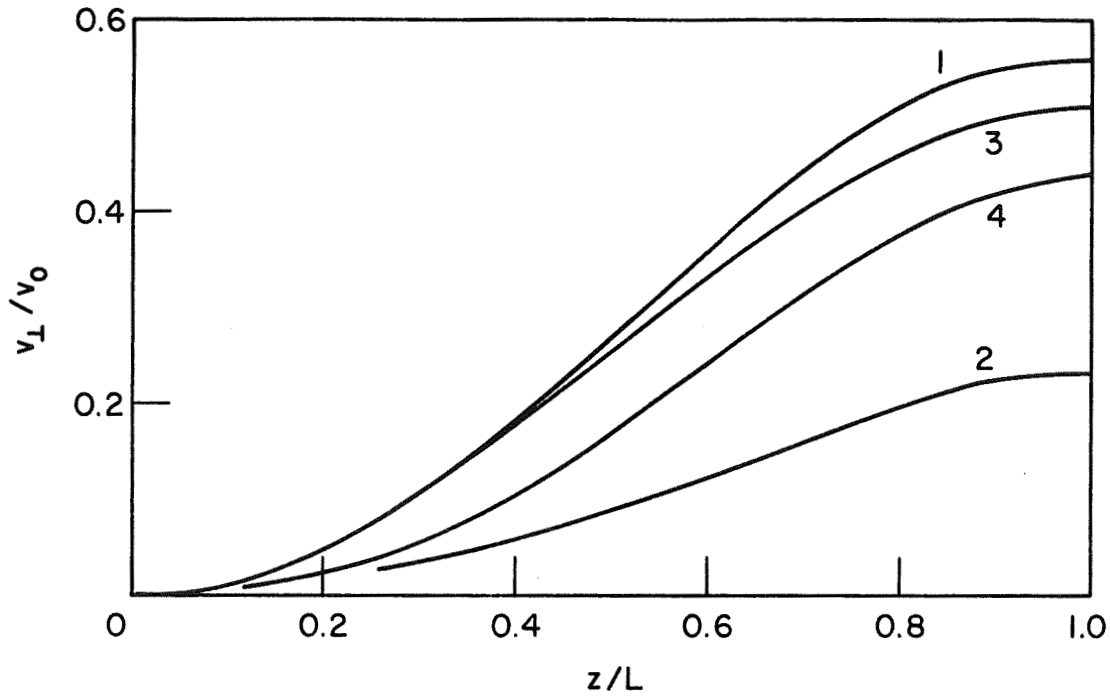


FIG. 3.2 (v_{\perp}/v_0) VS. z/L FOR PARTICLES WITH DIFFERENT INPUT PHASE ANGLES χ_0 .



- (1) $B_z = B_0; \chi_0 = 0$ DEGREES
- (2) $B_z = B_0; \chi_0 = 72$ DEGREES
- (3) $B_z = 0.96 B_0; \chi_0 = 0$ DEGREES
- (4) $B_z = 0.96 B_0; \chi_0 = 72$ DEGREES

FIG. 3.3 EFFECT OF VARIATION OF AXIAL MAGNETIC FIELD STRENGTH ON VELOCITY SPREAD. (B_0 IS THE DESIGN VALUE OF THE AXIAL FIELD STRENGTH AND χ_0 IS THE INPUT PHASE ANGLE OF THE PARTICLE.)

The curves 3 and 4 show the behavior of the same two electrons when the axial magnetic field is reduced by 4 percent from its design value. In this case the transverse velocities of the two particles are seen to be in the ratio of 1:1.14. This effect appears as a tuning effect in the experiment, where it is found that changes of only a few percent in the corkscrew current cause a sharpening of the velocity distribution.

The experimental setup for the study of cyclotron harmonic waves has been fabricated and installed in the vacuum system. A brief sketch of the apparatus is given in Fig. 3.4. An electron beam produced by the electron gun (A) is passed through the corkscrew device (B) which will convert 0.7 of its axial velocity into transverse velocity. The beam is then passed through a split-ring microwave coupler (C) and is allowed to drift through a slotted metallic cylinder (D). Three traveling probes (P_1, P_2, P_3) spaced 120 degrees apart around the circumference of D are used to study the dispersion characteristics of the waves launched on the beam. After passing through this drift space the beam passes through an output microwave coupler (E) and goes to the collector assembly (F). The collector assembly includes the pinhole beam analyzer used in our previous experiments. A suppressor grid to suppress the secondary electrons from the collector has been introduced. The microwave couplers (C,E), the drift cylinder (D) and the collector assembly (F) are held in their place by three slotted ceramic tubes which also act as guides for the coaxial probes. Each probe is capable of 2 inches of axial movement so that the entire 6-inch drift length can be scanned with the help of the three probes. The probe movement in vacuum is accomplished through the use of bellows and pulleys and is motorized.

3.3 Program for the Next Period. The experimental setup described above will be used for the study of dispersion characteristics and possible

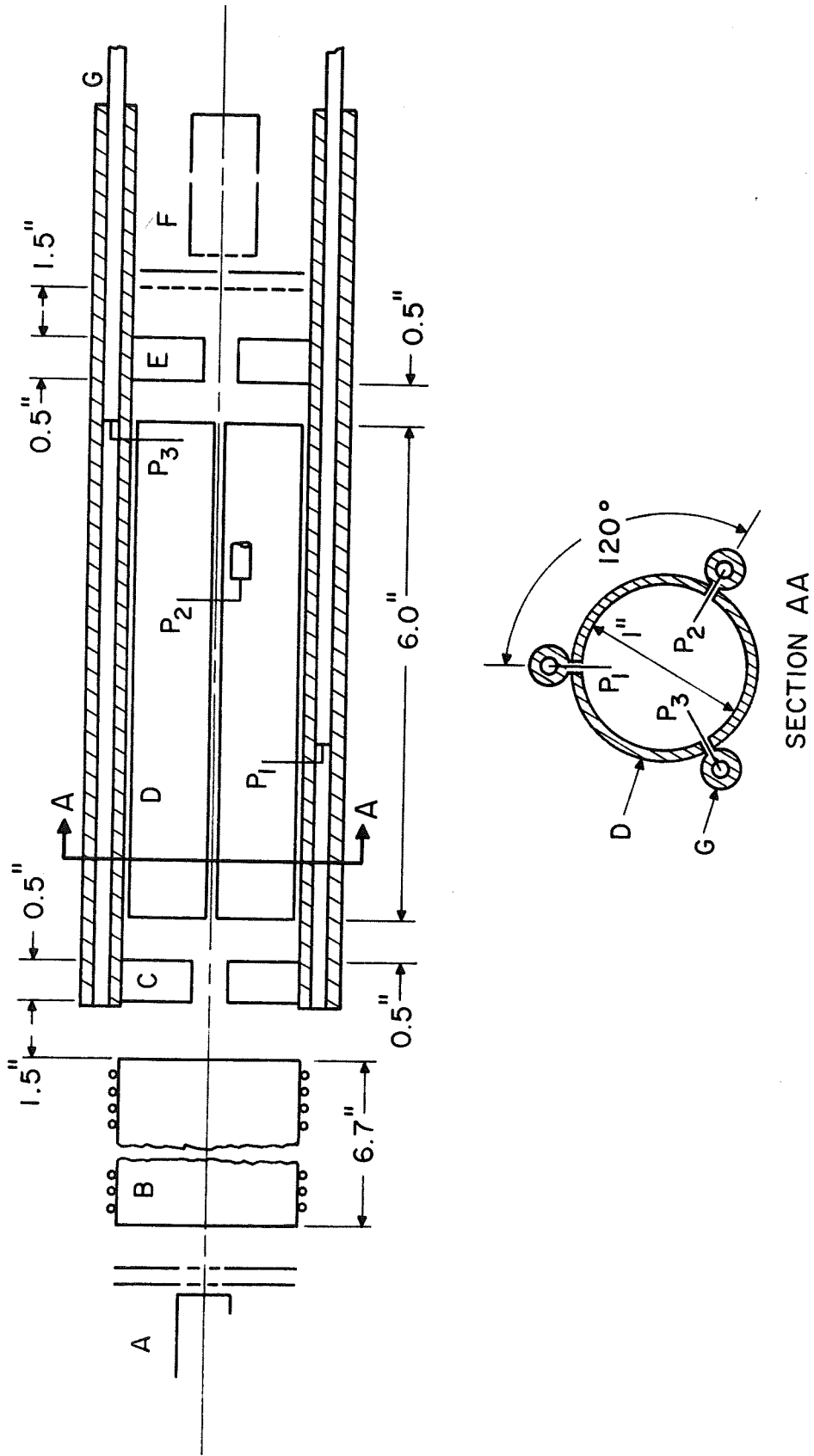


FIG. 3.4 THE EXPERIMENTAL SETUP FOR THE STUDY OF CYCLOTRON HARMONIC WAVES.

instabilities of the cyclotron harmonic waves. The velocity analyzer will be used to obtain more information about the beam velocity distribution. A digital computer program is under preparation to obtain more precise information about the conversion characteristics of the corkscrew device.

4. Paramagnetic Materials for Millimeter- and Submillimeter-Wave Detection

Supervisor: G. I. Haddad

Staff: C. F. Krumm

4.1 Introduction. The work on this phase of the program has been completed and a technical report on the results of this study is now being prepared. The abstract of this report appears below. This will also be Mr. Krumm's Ph.D. dissertation.

4.2 Abstract of Forthcoming Technical Report. "The purpose of this study is to investigate the use of paramagnetic materials for downconversion of millimeter- and submillimeter-wave radiation to microwave frequencies. The conversion scheme studied here utilizes three energy levels associated with the ground state of the paramagnetic material. Two of these levels are separated by a microwave frequency and two by a millimeter-wave frequency. Power applied at the millimeter-wave frequency causes the spin population to redistribute itself among the levels and causes a corresponding change in the power absorbed at the microwave frequency. The overall effect is that changes in the millimeter-wave power level cause corresponding changes in the microwave power absorption.

"The downconversion process is analyzed using a microscopic approach. The results of this analysis indicate that the downconversion loss is minimized when the microwave input power approaches the saturation level. Under these conditions the microscopic conversion loss approaches the fundamental limit which is the ratio of the microwave frequency to the

millimeter-wave frequency. The response time of the downconverter is also shown to improve with increasing microwave power input. Both of these predictions have been verified experimentally.

"The microscopic results are used to develop an equivalent circuit for the downconverter. This circuit is used to analyze the downconverter performance. The dependence of the conversion loss on mismatch, frequency and magnetic field tuning, and saturation is determined. The minimum detectable millimeter-wave input power when a given type of microwave receiver is employed is also evaluated. It is shown theoretically and has been verified experimentally that the minimum detectable power exhibits a minimum as a function of the microwave input power level.

"An experimental program was undertaken to demonstrate the feasibility of using downconversion as an alternative to direct detection at millimeter- and submillimeter-wave frequencies. Using iron-doped rutile as the conversion medium, downconversion has been achieved at both liquid nitrogen and liquid helium temperatures. The experimental performance of this device is in substantial agreement with the theoretical predictions. Terminal to terminal conversion losses as low as 15 dB were observed at liquid helium temperatures. The observed response times were on the order of milliseconds at 4.2°K and tens of microseconds at 77°K. The noise equivalent power observed in these initial experiments indicates that the sensitivity of this device is comparable to that of a video detector. The major portion of the work was carried out at 35 GHz where equipment was available. The microwave signal is at 9 GHz. The measured noise equivalent power on the present system was approximately -70 dBm. By proper design of the system this can be reduced to approximately -90 dBm."

4.3 Program for the Next Period. A new scheme which utilizes four energy levels instead of three where some of the limitations in the three-level scheme can be eliminated will be investigated. This will be described in detail in the next report.

5. Bulk Semiconductor Materials for Millimeter- and Submillimeter-Wave Detection

Supervisor: G. I. Haddad

Staff: I. I. Eldumiati

This part of the program is concerned with the properties of bulk semiconductor materials which are suitable for applications in the millimeter- and submillimeter-wave regions. Cavity perturbation techniques using field theory and equivalent circuit analyses are being used for this purpose. The field theory approach was outlined in the last progress report.

An equivalent circuit of the bulk material in a reentrant cavity was developed. The equivalent circuit was used to express the frequency shift and the change in the coupling factor of the cavity as a function of the material and the cavity parameters. This model is being used to study the material interaction with electric and magnetic fields as a function of temperature. A computer program has been written to study the coupling problem, the optimum operating points and to interpret the experimental results.

A new experimental cavity system was designed and is being constructed. This setup will eliminate all cooling problems and provide means to change the coupling to the cavity at X-band and higher frequencies. It also allows testing of the feasibility of the detection scheme outlined in Semiannual Progress Report No. 3.

In the next period the theoretical investigation of the complex dielectric constant and its dependence on temperature, electric and magnetic

fields will be continued. Experiments at X-, Ku- and E-bands will be carried out at liquid nitrogen and liquid helium temperatures. The feasibility of millimeter-wave detection in InSb will be tested.

6. Millimeter-Wave Gunn-Effect Devices

Supervisor: W. R. Curtice

Staff: J. J. Purcell

6.1 Introduction. In the last report a phenomenological rather than microscopic analysis of the ISA-mode Gunn effect in gallium arsenide was described. Solutions for bulk negative conductivity, including energy relaxation effects, were obtained and the results were shown to be compatible with those of other workers. The analysis assumed a uniform field distribution throughout the semiconductor whereas in a practical device, field nonuniformity may be caused by an accumulation of carriers or by a permanent nonuniformity in donor doping density.

The most basic space-charge instability is a pure accumulation layer. High-velocity, low-field carriers on the cathode side feed the negative charge layer, while low-velocity electrons on the anode side inhibit charge depletion. This convectively amplifying space-charge perturbation will occur even in the case of a perfect crystal due to the field gradient at the crystal's cathode interface. In addition, local perturbations in the negative-conductivity region will give rise to growing high- and low-field domains.

The effects of a traveling charge accumulation layer and a dynamic high-field domain have been incorporated into the theoretical model. The model is described briefly and results of calculations for a few specific cases are discussed.

6.2 Dynamic Accumulation Layer. The analysis previously reported showed that by taking a sufficiently large number of discrete time intervals,

a closed-loop solution could be obtained for the average electron drift velocity as a function of the cyclic electric field variation. The crystal is now considered to be divided into two sections by a thin accumulation layer as indicated in Fig. 6.1. The average electron velocities are calculated for both the cathode and anode sections as the accumulation layer drifts through the crystal. Charge growth or decay is determined by solution of Poisson's equation, the equation of continuity and the total device voltage. After adding the conduction and displacement currents in either of the sections, values of conductance, susceptance and efficiency are obtained by Fourier analysis of the total device current. In Fig. 6.2, the drift velocity for each section of a 50 μm crystal is shown as a function of electric field for a dc bias field of 10 kV/cm and an RF field of 7.7 kV/cm at 7 GHz. The dashed and continuous curves represent the path followed in the anode and cathode sections, respectively.

In order that the solution should be cyclic, it is essential that the accumulation layer be completely quenched during the RF cycle. A parameter which controls the growth and decay of the accumulated charge is the ratio of carrier density to frequency, n_0/f . By calculation over a wide range of frequencies, lengths and doping densities, minimum values of n_0/f were determined. These values lay within the limits estimated by Copeland¹ for possible LSA operation.

6.3 Dynamic-Domain Formation. Following the inclusion of an accumulation layer in the model, attention was directed to studying the effect of a small notch in the background donor density. The electric field pattern assumed is shown in Fig. 6.3. Solution of a differential equation

1. Copeland, J. A., "LSA Oscillator-Diode Theory," J. Appl. Phys., vol. 38, No. 8, pp. 3096-3101, July 1967.

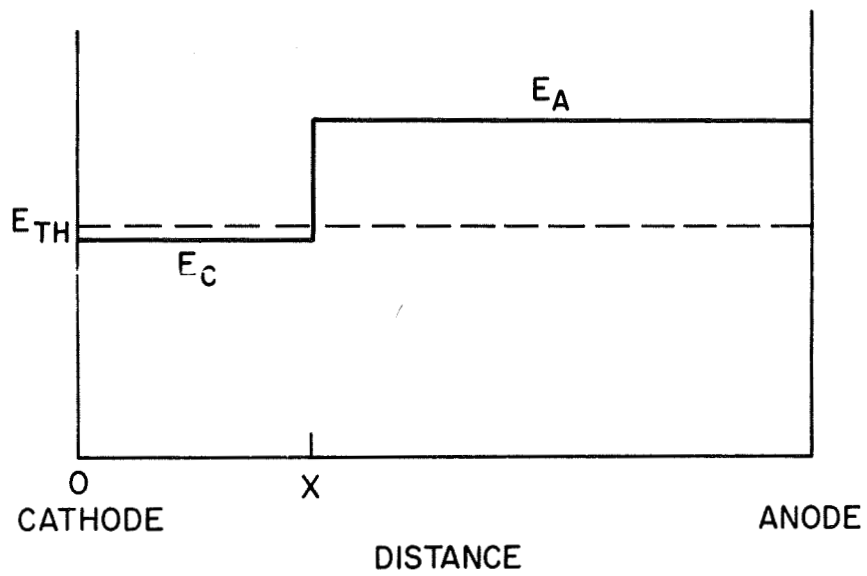


FIG. 6.1 ELECTRIC FIELD CONFIGURATION IN THE MODEL CRYSTAL
SHOWING THE ANODE, CATHODE AND THRESHOLD FIELDS;
 E_A , E_C AND E_{TH} , RESPECTIVELY.

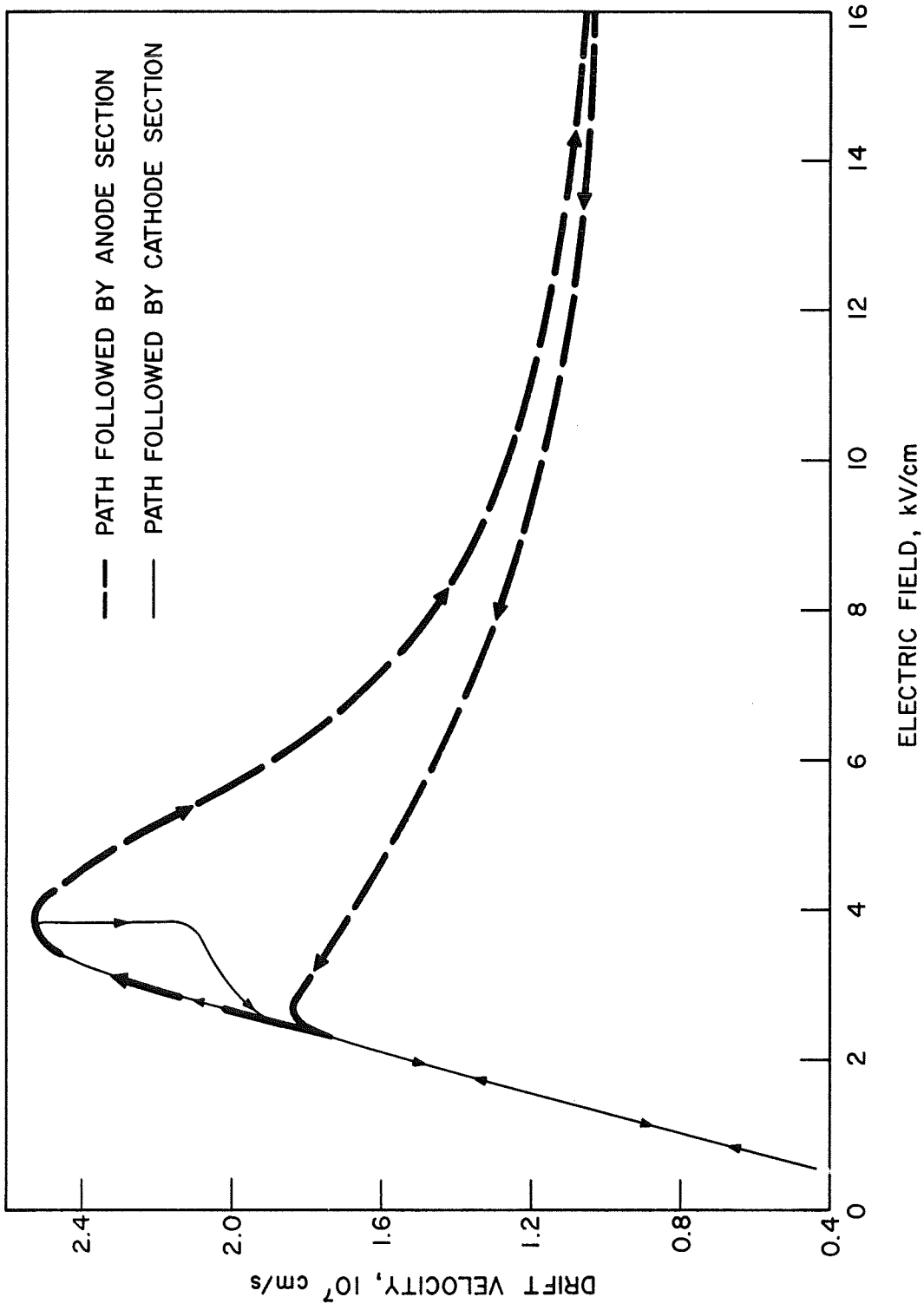


FIG. 6.2 AVERAGE ELECTRON DRIFT VELOCITIES AS A FUNCTION OF ELECTRIC FIELD IN THE ANODE AND CATHODE SECTIONS OF THE CRYSTAL.

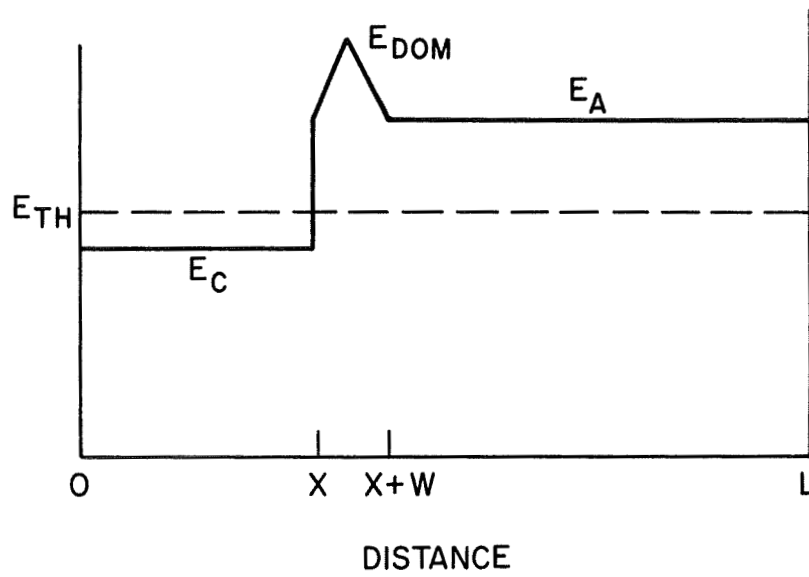


FIG. 6.3 ELECTRIC FIELD CONFIGURATION IN THE MODEL CRYSTAL WITH A HIGH-FIELD DOMAIN INCLUDED.

derived from Poisson's equation and the continuity equation, including diffusion, yielded a value for the initial domain voltage corresponding to a particular doping notch. As the field in the anode section exceeds threshold, the domain voltage grows at an exponential rate determined by the slope of the v-E curve. For larger domain voltages, the growth rate is determined by the integral expression of Kurokawa² (Eq. 4), which describes domain growth and decay. The domain continues to grow until the outside field falls below threshold and domain quenching occurs.

As the domain voltage increases, so does the domain width as shown by Butcher et al.³ When the domain width fills the anode section, the device can no longer be an LSA oscillation, and some other mode of oscillation may result. This condition imposes a maximum limitation on the value n_0/f .

6.4 Theoretical Results. Figure 6.4 shows efficiency as a function of n_0/f for a bias field of 10 kV/cm, a crystal length of 50 μm and a doping density of $10^{15}/\text{cm}^3$. Two cases are shown, corresponding to 1 and 3 percent doping density notches, 2 μm in length.

Values of n_0/f less than the lower limits indicated on the curves would leave an unquenched accumulation of charge at the end of the RF cycle, whereas too large an n_0/f value causes the domain to grow to a width exceeding the anode section of the crystal. As the RF electric field is increased, the permissible n_0/f range is extended but efficiency is reduced. A 3 percent doping fluctuation is probably less than is normally present in any crystal.

-
2. Kurokawa, K., "The Dynamics of High Field Propagating Domains in Bulk Semiconductors," Bell System Tech. J., vol. XLVI, No. 10, pp. 2235-2259, December 1967.
 3. Butcher, P. N., Fawcett, W. and Ogg, N. R., "Effect of Field Dependent Diffusion on Stable Domain Propagation in the Gunn Effect," Brit. J. Appl. Phys., vol. 18, No. 6, pp. 755-759, June 1967.

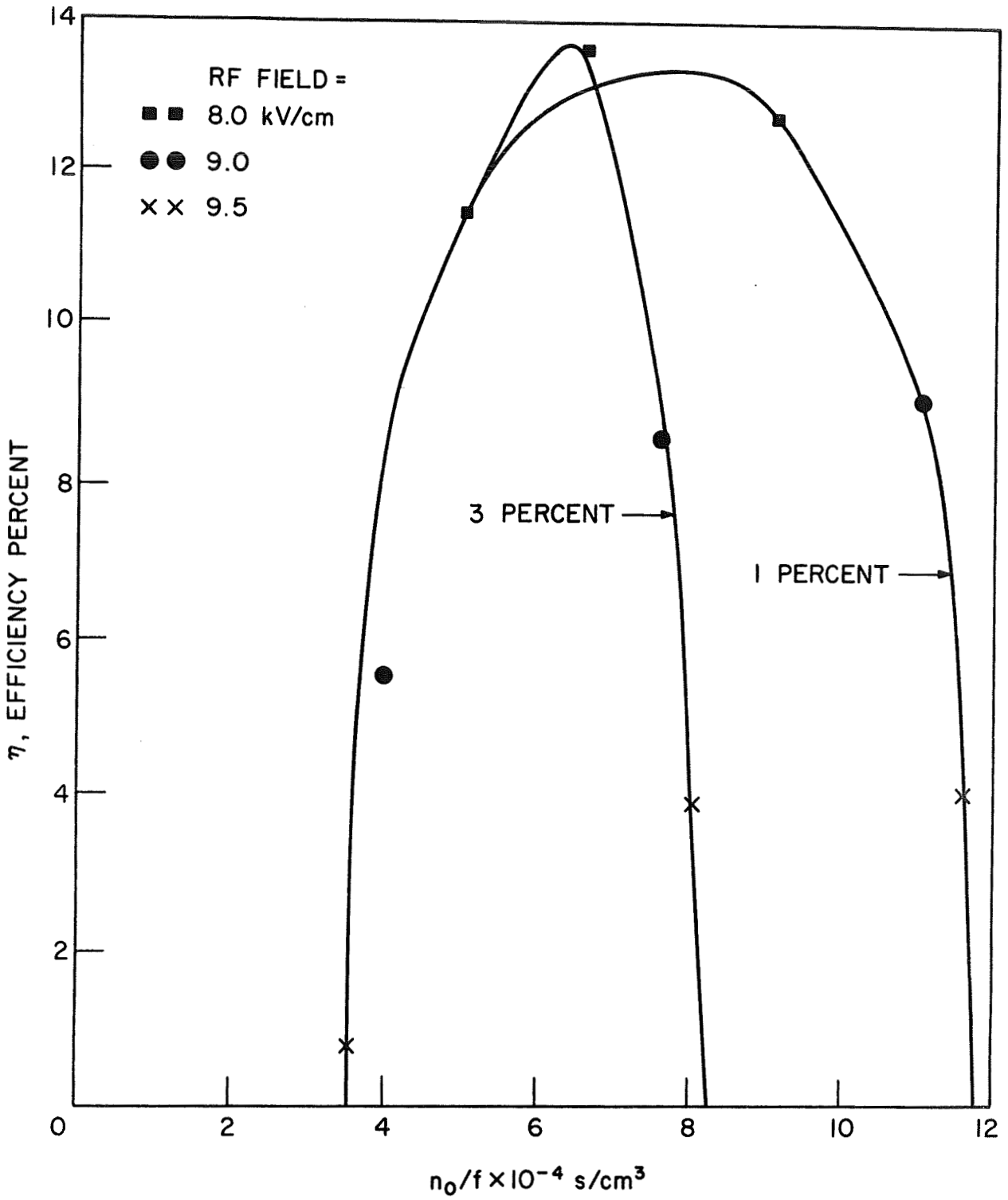


FIG. 6.4 EFFICIENCY AS A FUNCTION OF n_0/f FOR VARIOUS VALUES OF RF FIELD. Dc BIAS IS 10 kV/cm, DOPING DENSITY IS $10^{15}/\text{cm}^3$ AND THE CRYSTAL LENGTH IS 50 μm . THE CURVES ARE PLOTTED FOR DOPING FLUCTUATIONS OF 1 AND 3 PERCENT.

In order to operate the device at higher doping fluctuations, a larger dc bias is necessary.

6.5 Experimental Study. During this period, a microwave circuit was designed and constructed for operation of gallium arsenide devices in Ka-band (26-40 GHz). The device is contacted by a bellows soldered to a central copper post in the E-plane of an RG/96U rectangular waveguide. Dc bias is provided through an OSM connector with an RF choke which touches the opposite side of the device. Tuning of the circuit is accomplished by an adjustable short circuit behind the crystal mount and an E-H tuner between the mount and the load.

Preliminary tests have produced 2 mW of power at 24 GHz using a commercially packaged 10.5 μm device, and 0.2 mW at 37 GHz with unpackaged epitaxial material of 20 μm length.

6.6 Conclusions. The theoretical model has been completed and initial calculations show that it does predict a restricted range of permissible values of n_0/f for ISA-mode operation. The Ka-band circuit for ISA tests was operated at 24 and 37 GHz and should prove useful for correlating the theoretical results with experimental tests.

6.7 Program for the Next Period. In the next period, ISA-mode calculations will be made for a wide range of parameters so that optimum operating conditions may be predicted for millimeter-wave power generation.

7. Analysis of Avalanche-Diode Oscillators

Supervisor: R. J. Lomax

Staff: M. S. Gupta

7.1 Introduction. The objective of this phase of the investigation is to analyze a realistic model of avalanche microwave diodes which would

explain some experimental observations and would lead to a better understanding of avalanche-diode oscillators. As described in the last progress report, the assumptions made explicitly or implicitly in the various analyses of avalanche-diode oscillators performed so far were critically examined. It was found that while certain assumptions made in the original analysis of Read regarding the width of the avalanche region, the magnitude of the ionization rate and the shape of the doping profile have been abandoned in favor of more realistic assumptions in subsequent analyses, some of the more basic assumptions have perpetuated which may be expected to have significant influence on the results.

All published analyses require the voltage across the semiconductor wafer to be specified and proceed from there to calculate the diode current by solving the carrier transport equations. One usually assumes a sinusoidal voltage, or a superposition of more than one sinusoidal voltage, while the calculated current has a large number of frequency components. Requiring self-consistency, one is led to assume that the circuit (including package) impedance is zero at all frequencies other than that (or those) at which the voltage was assumed to be present initially. Such an assumption seems undesirable for two reasons: (1) The admittance of the diode at one frequency is affected strongly by the presence of other frequencies.¹ (2) Higher efficiencies are attainable by intentionally making the circuit resonant at more than one frequency.²

-
1. Schroeder, W. E., Greiling, P. T. and Haddad, G. I., "Multifrequency Operation of IMPATT Diodes," To be presented at the 1969 IEEE Int. Electron Devices Meeting, Washington, D. C., October 1969.
 2. Swan, C. B., "IMPATT Oscillator Performance Improvement with Second Harmonic Tuning," Proc. IEEE, vol. 56, No. 9, pp. 1616-1617, September 1968.

7.2 Analysis. An entirely novel method was used to solve for the voltage across the diode and the current through it in a self-consistent manner. Circuit parameters were measured for some actual avalanche-diode circuits and the circuit admittance was calculated over a wide frequency range (from less than 80 MHz to above 20 GHz), assuming the absence of higher-order modes in the coaxial-line circuit. Then the carrier transport equations for a Read model of the diode³ were solved in an iterative manner requiring the voltage and current for the diode to be related to each other through the circuit admittance.

7.3 Conclusions. It was found that the waveform of the voltage across the diode is strongly dependent upon the circuit connected across the diode. The effect can be explained in terms of admittance plane plots for the circuits. A separate report on this portion of the work is presently being prepared.

7.4 Program for the Next Period. A few computer runs will be made to finalize the results of this part of the work for incorporation into a technical report.

3. Read, W. T., "A Proposed High-Frequency, Negative-Resistance Diode," Bell System Tech. J., vol. 37, No. 2, pp. 401-446, March 1958.